# CERVICAL BRACHYTHERAPY WITH YTTERBIUM-169

Major Qualifying Project Report

Submitted to the Faculty of

WORCESTER POLYTECHNIC INSTITUTE

In partial fulfillment of the requirements for the

Degree of Bachelor of Science

by

Sergey Korkhov

## Abstract

High-dose rate brachytherapy is a type of treatment of cancer whereby a radioactive source is inserted directly into the tissue or its nearest vicinity for short time intervals, damaging the DNA of rapidly dividing cancer cells and triggering cell death. This study considers Ytterbium-169, a high-energy photon source, as an alternative to Iridium-192, the current HDR brachytherapy standard. We demonstrate that Ytterbium-169 performs as successfully as Iridium-192 in delivering a high, uniform dose to soft tissues, but results in an unfavorably high dose to bone tissue. We suggest that Ytterbium-169 is a promising target for intensity modulated brachytherapy.

**Table of Contents:**

# 1 ACKNOWLEDGEMENTS

I would like to give my sincerest thanks to my MQP advisor, Professor David Medich for his feedback through the project. This project would not be possible without his keen guidance and advice. I would also like to thank my friends and family who believed in me and supported me along the way.

# 2 INTRODUCTION

## 2.1 PURPOSE

The purpose of this work is to explore the use of Ytterbium-169 as a source for cervical brachytherapy with the goal in increasing the ratio of the dose delivered to the tumor to the dose absorbed by surrounding healthy tissues. In particular, this work uses a Monte Carlo simulation to compare the outcomes of using Ytterbium-169 to those achieved with the current industry standard, Iridium-192 (Lawrence *et al.*, 2008).

## 2.2 BRACHYTHERAPY

### *2.2.1 BACKGROUND*

Cervical cancer is the third most common cancer in the United States, with 12,820 estimated new cases and 4,210 estimated deaths in 2017 (U.S. Cancer Statistics Working Group, 2016). The 5-year survival rate for women affected by cervical cancer varies between 91% for women diagnosed at an early stage to 17% for those with late-stage tumors, resulting in an overall 5-year survival rate at 68% (U.S. Cancer Statistics Working Group, 2016). Radiotherapy remains one of the most effective treatments for cervical cancer and, as it is currently used to treat both early-stage (IA2) and advanced cervical cancers, it is one of the most commonly used treatments for the condition (American Cancer Society, 2016)

### *2.2.2 GENERAL APPROACH*

Brachytherapy is a type of cancer treatment delivered by insertion of an encapsulated radioactive source into the tissue of a tumor. Brachytherapy is used for a number of different cancers, including cervical, breast, prostate, eye, and brain cancers. An internal radiation therapy,

brachytherapy is applied in conjunction with external beam radiation therapy and is generally subdivided into a low-dose rate (LDR) and high-dose rate (HDR) brachytherapy.

HDR brachytherapy is delivered via insertion of cylindrical encapsulated pellets - "seeds" - into a cavity near the tumor or into the tumor directly through a plastic tube, using a steel wire attached to the pellet as a guiding device. The sources are packaged into small stainless steel capsules, and reach the size of a grain of rice. To control for differences in sources' energies, and activities, a dose prescription convention is adopted. For brachytherapy of cervical cancer, considered this report, the International Committee on Radiation Units and Measurements' Report 38 (ICRU38) outlines the most commonly applied approach to prescribing radiation doses to point in the in the treatment site (International Committee on Radiation Units and Measurements, 1985; Banerjee and Kamrava, 2014) The radiation dose in prescribed to point A – a point located 2 cm upwards along the main axis of the cylindrical source, and 2 cm lateral to the axis. Thus, prescription point A is removed from the seed by $r_A \approx 2.83$ cm.

### *2.2.3 General Principle*

The primary type of radiation responsible for delivering prescribed doses to tissues is radiation emitted from the sources in the form of high-energy photons – x-rays and gamma-rays (Lawrence *et al.,* 2008). Although many medical radiation sources emit electrons, the Coulomb interactions that result from non-zero charge, and low energy does not allow them to travel through the tissues to an appreciable extent and, as a result, causes the electrons to deposit their energy locally, where the first interaction event between the electron and an atom of the tissues occurs (Jawett and Serway, 2008). High-energy photons, on the other hand, penetrate matter to a much greater extend, and are able to deposit their energy over longer distances. Thus, with

respect to brachytherapy, high-energy photon-tissue interactions decide the therapeutic outcomes. It is, therefore, these interactions that this paper discusses.

Although the primary focus of this work is HDR brachytherapy, the same physical principles guide the effects of all aforementioned brachytherapy types on tissues of the body. Photons emitted from a source, can interact with the atoms of the body tissues in one of three ways:

1. Photoelectric effect
2. Compton scattering
3. Electron-positron pair production.

Two factors affect the type on interaction between the body tissues and the photons:

1. The energies of photons produced by medical nuclides fall in the range between 21 keV for relatively low-energy Palladium-103, to 3500 keV for high-energy Ruthenium-106 (Rijnders, 2009).
2. The tissues of the body are comprised primarily of elements with average atomic numbers of $Z_s = 7.5$ for soft tissue (dominant elements $_6$C, $_7$N, $_8$O) and $Z_b = 13$ for bone (dominant elements $_6$C, $_8$O, $_{15}$P, $_{20}$Ca).

As Figure 1 suggests, the energies of incident photons and atomic numbers of most common biological elements point at Compton scattering as the characteristic process that dominates in high-energy photon interactions with body tissues.

### *2.2.4 Compton Scattering*

Compton scattering is a type of inelastic photon scattering that occurs between a charged particle – an electron, in the case of brachytherapy – and a photon, and result in a decrease of photon

energy and ionization of the electron-bearing atom. The increase in the photon wavelength associated with the energy loss is given by the famous relation due to Compton (Jawett and Serway, 2008):

$$\lambda' - \lambda = \frac{h}{m_e c}(1 - \cos(\theta))$$

where

$\lambda$ - photon wavelength before scattering,

$\lambda'$ - photon wavelength after scattering,

$\theta$ - scattering angle, i.e. angle between the directions of scattered and incident photon

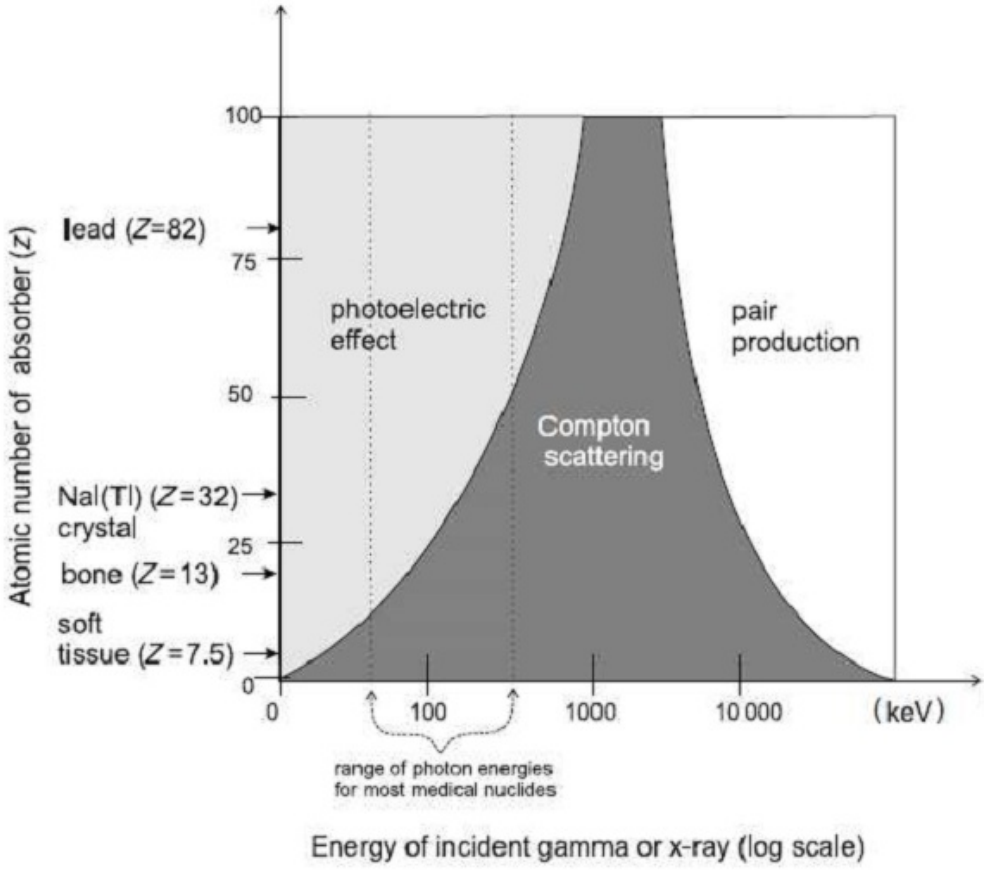


**FIGURE 1. TYPE OR INTERACTION THAT OCCURS BETWEEN AN X-RAY OR GAMMA-RAY SOURCE AND ATOMS OF DIFFERENT ATOMIC NUMBERS.**

$m_e$ - electron mass

$c$ - speed of light in vacuum

$h$ - Plank's constant

The energy of the scattered photon is given by

$$E' = \frac{E}{\frac{E}{m_e c^2}(1 - \cos(\theta)) + 1}$$

where $E$ is the energy of incident photon.

Therefore, during Compton scattering, the energy of supplied to an electron in the atom is given by the following equation:

$$\Delta E(E, \theta) = E - E' = \frac{E(1 - \cos(\theta))}{1 - \cos(\theta) + \frac{m_e c^2}{E}}$$

The probability that a particular photon with energy $E$ incident onto an electron will scatter at a specific angle $\theta$ while supplying energy $\Delta E$ to the electron is given by Klein-Nishina distribution. Since scattering is fundamentally a quantum-mechanical event, the exact energy left to an electron cannot be predicted exactly for any individual interaction.

It is clear, however, that the energy of an electron after Compton scattering cannot exceed the energy of the incident photon. Therefore, after ionization from Compton scattering with high-energy photons produced by most medical radiation sources, ejected electrons will have energies no more than approximately 1 MeV. Supplied with this energy, electrons will travel over a distance of under 5 mm before depositing all of their energy in the tissue. Given the Iridium-192 and Ytterbium-169 average photon energies of 387.5 keV and 92.7 keV, respectively, electrons

will deposit their energy over even smaller distances (Rijnders, 2009; Chu *et al.,* 1999). Thus, for the purposes of the paper, all traveling electrons are assumed to deposit their energy locally, as stated above.

### *2.2.5 PHOTOIONIZATION*

In addition to Compton scattering, photons with energies below 100 keV can interact with heavier elements of the body, such as $_{15}$P and $_{20}$Ca particularly abundant in bones and result in photoionization of atoms of those elements. In this case, a photon will be fully absorbed, and an electron will be ejected from the atom participating on the interaction (Jawett and Serway, 2008). For the reason given above, this will result in all of the photon energy being deposited locally, at the site of interaction.

### *2.2.6 IRIDIUM-192*

Currently, the standard source for HDR cervical brachytherapy is Iridium-192 (Table 1). The energies and intensities of photons emitted by Iridium-192 are given in blue in figure Figure 2. Iridium-192 is produced from iridium metal by neutron activation in nuclear reactors. Its energy spectrum and high specific activity makes it a good source for HDR brachytherapy: (Lawrence *et al.,* 2008)

1. Iridium photons interact with tissues via Compton scattering and are not energetic enough to travel unobstructed delivering excessive dose to healthy tissues
2. A small Iridium-192 source is capable of delivering high enough dose rate necessary for HDR brachytherapy.

**TABLE 1. PHYSICAL PROPERTIES OF IRIDIUM-192 (MEDICH AND MUNRO, 2007).**

| Iridium-192 Physical Properties | |
|---|---|
| Half-life | 73.8 days |
| Decay Mode | $\beta, \gamma, \varepsilon$ |
| Production mode | Thermal Neutron Activation |
| Average energy | 387.5 keV |

### *2.2.7 YTTERBIUM-169*

Ytterbium-169 – a radioactive isotope of Ytterbium. Produced similarly to Iridium-192, but displays a different radiation spectrum. Most of its photon energies are in the range between 40 and 100 keV, with the most intensive photon emitted with an energy of 50.7 keV. The average energy of Ytterbium-169 photon spectrum is 92.7 keV – more than 4 times lower than that of Iridium-192. Yet, as the energies of Ytterbium-169 photons fall in the range described above, Compton scattering still remains the characteristic interaction type between Ytterbium-169 photons and tissues of the body allowing the material to distribute the radiation dose in a way similar to Iridum-192 (Medich *et al.,* 2006)

Similar to Iridium-192, Ytterbium-169:

1. Delivers the dose via Compton scattering and absorption of high-energy photons in the tissues of the body.
2. Has high specific activity and is capable of delivering high dose rate necessary for HDR brachytherapy.

Due to its lower energy spectrum, Ytterbium-169 possesses the following advantages over Iridium-192 for HDR brachytherapy:

1. Ytterbium is more easily shielded and is safer to handle.
2. Ytterbium can be combined with intensity modulation techniques such as partial seed shielding to improve the dose control.

**TABLE 2. PHYSICAL PROPERTIES OF YTTERBIUM-169 (MEDICH *ET AL.*, 2006)**

| Ytterbium-169 Physical Properties | |
|---|---|
| Half-life | 32 days |
| Decay Mode | $\varepsilon$ |
| Production Mode | Thermal Neutron Activation |
| Average energy | 50.7 KEV |

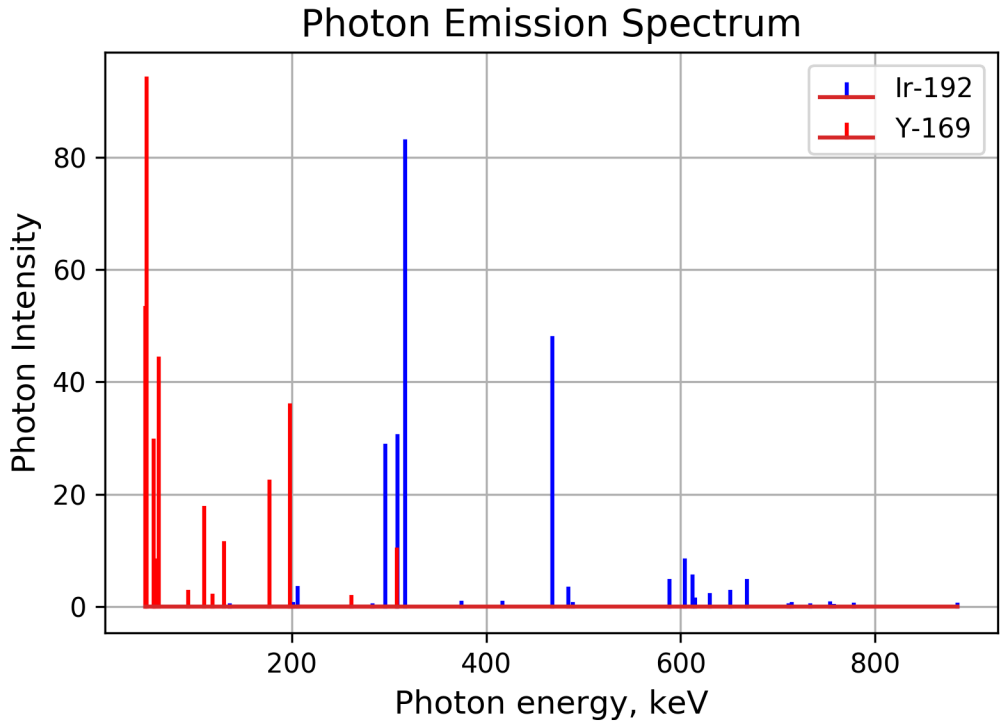


**FIGURE 2. PHOTON EMITTION SPECTRUM OF YTERBIUM-169 (RED) AND IRIDIUM-192 (BLUE) WITH RELATIVE INTENSITIES. AS SEEN ON THE GRAPH, YTTERBIUM SPECTRUM LIES ALMOST ENTIRELY IN THE LOWER ENERGY REGION THAN THAT OF IRIDIUM, WITH THE MOST INTENSIVE PEAR AT 50.7 KEV. IRIDIUM, ON THE OTHE HAND, EMITS PHOTONS OF HIGHER ENERGIES, WITH THE MOST PROMINENT PEAK AT 316.51 KEV. (CHU ET AL., 1999)**

### *2.2.8 PROBLEM STATEMENT*

It has been shown that increased dose to the prescription point A correlates with an increased local control over the tumor, and, therefore, improved clinical outcomes (Eifel *et al.,* 1994). Meanwhile, an increased dose to the prescription point is traditionally associated with a higher dose to the healthy tissues surrounding the tumor (Lawrence *et al.*, 2008). Hence, finding ways to increase the dose delivered to the prescription point without the toll of overdosing the tissues

outside the target is an attractive objective in brachytherapy research. Having introduced two radiation sources, Iridium-192 currently used for HDR brachytherapy and Ytterbium 169, this study models the use of Ytterbium-169 for HDR brachytherapy and compares the outcomes to the use of Iridium-192.

## 2.3 MODELING

To be applicable, the model of the problem had to simulate the following elements of the process:

1. *Female anatomy and tissue arrangement.* Cervical brachytherapy targets specific volumes within female anatomy that span different tissues with varied elemental composition. Brachytherapy seeds are placed at specified location within the geometric framework defined by the anatomy, and the photons emitted from the sources interact differently with tissues with different elemental compositions. The simulation had to accounted for the complex arrangement of materials inside the body.
2. *Radioactive sources.* The simulation had to include radiation sources of proper sizes, geometries, and composed of specified material with known decay modes and emission spectra.
3. *Interactions between emitted particles and body tissues.* The simulation had to model primary photon-tissue interactions between the photons emitted from the seed and atoms of the surrounding tissues, as well as particles produced as a result of the interactions.

Since each source photon participates in numerous interactions during its lifetime, Monte Carlo method was used to model the problem.

### *2.3.1 MONTE CARLO METHOD*

Monte Carlo method is a numerical technique particularly effective to solve model statistical processes – processes with outcomes determined by random sampling from a probability distribution. The method is frequently applied to problems involving large numbers of statistically determined events. Due to the large number of particle-particle interactions involved in modeling brachytherapy, and due to the probabilistic outcomes of those interactions, Monte Carlo model was used to model the treatment.

During the Monte Carlo simulation, each of the following physical parameters is sampled from their respective distributions ($i$ - particle index)

1. $\boldsymbol{r}_{i,o}$ - starting position of the particle within the source
2. $\boldsymbol{v}_{\mathrm{i},0}$ - initial velocity of the particle
3. $d_{i,\boldsymbol{r}}$ - distance traversed before the next interaction, depends on the medium
4. $\boldsymbol{v}_{i,\boldsymbol{r}}$ - "new" velocity of the particle after the interaction,

   where $\boldsymbol{r}$ is coordinate vector of the point where the particle interacts with the surrounding matter.

In addition to the parameters above, the type of interaction that occurs at position $\boldsymbol{r}$ is also determined probabilistically and depends on the energy of the particle being tracked and the particle with which it interacts. In this manner, Monte Carlo algorithm resamples the parameters of interest to construct the particles' trajectory, segment by segment.

In terms of modeling brachytherapy, the Monte Carlo method entails the following steps:

1. Generate a photon at a point within the volume of the source with a starting energy drawn from a discrete distribution shown in Figure 2.

2. Sample the distance traveled by the photon before interaction. Determine the type of interaction from a distribution. For all particles that exist after the interaction, i.e. scattered photons and/or ejected electron, repeat the steps to determine all trajectory segments for all generated particles to the boundary of the problem space.

The Monte Carlo method generates a large number of instances of the physical process, such as photons leaving the radiation source, and computes the average of the parameter on interest, e.g. dose rate delivered to a voxel of the model.

### *2.3.2 Monte Carlo N-Particle Transport (MCNP) Code*

MCNP6 Code is an implementation of the Monte Carlo method designed specifically to model nuclear events, transport, and interactions of subatomic particles developed at Los Alamos National Laboratory (LANL). MCNP6 allows the user to define the following problem parameters (Goorley *et al.,* 2012):

1. Problem universe
    a. Geometry (i.e. anatomy) of bodies in the problem, such as the anatomy and sources of radiation. Surfaces separating the 3D volumes are defined defined by second degree elliptic and fourth degree toroidal surfaces. Volumes in geometry are defined with union and intersection logical operators.
    b. Elemental composition of materials that make up the geometry, i.e. the elemental composition of tissues of the body.
    c. Density of the materials in the problem geometry.
2. Radioactive source
    a. Radiation spectrum

    b. Source placement

3. Dose tally
    a. Method to count contributions from modeled particles
    b. Type of contributions (e.g. dose rate)
4. Simulated physics of interactions
    a. Type on interaction that are allowed to happen in the simulation.

The details of using the MCNP6 Code can be found in the MCNP6 User Manual (Goorley *et al.,* 2012) and are beyond the scope of this report.

The MCNP6 Code was used as the modeling software because:

1. Frequently used for simulation in medical physics;
2. Provides extensive libraries with material properties;
3. Describes physical interaction that occur in the energy range between 10 keV and 1000 keV, which encompasses the energy range of the interaction from Iridium-192 and Ytterbium-169 brachytherapy sources;
4. Provides an industry-standard phantom of an adult female – MIRD Phantom (Xu and Exkerman, 2009) – necessary for cervical HDR brachytherapy simulations.

### *2.3.3 MIRD PHANTOM*

The MIRD Phantom developed by Eckerman et. al is a simplistic model of a female human body. The Phantom consists of 35 discrete cells – organs – filled with one of the 4 types of media: air, soft tissue, bone tissue, or lung tissue. Cross-sectional images of the model implemented in the MCNP Code are shown in Figures 3 and 4.

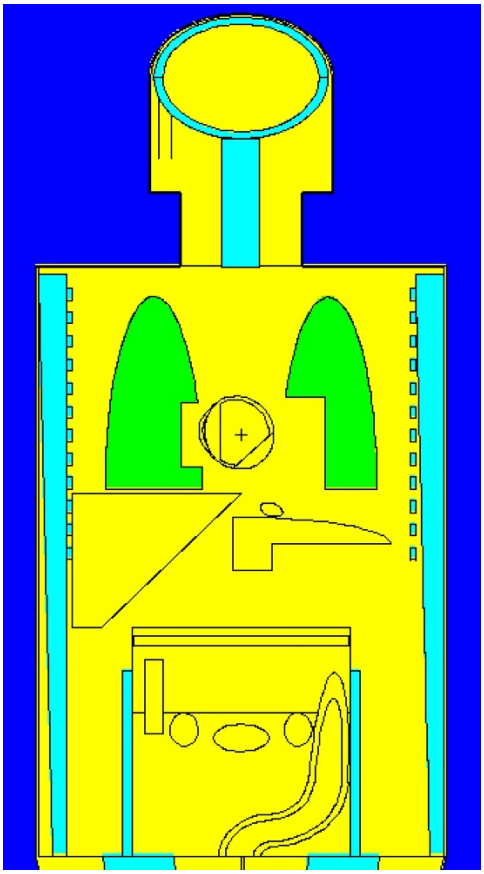

**FIGURE 3. FRONTAL VIEW OF THE MIRD PHANTOM TORSO. YELLOW - SOFT TISSUE, GREEN - LUNG TISSUE, TURQUOISE - BONE TISSUE, BLUE - AIR.**

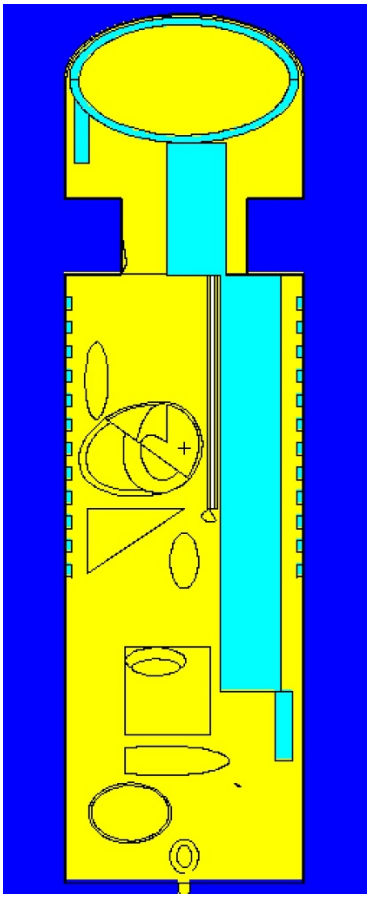

**FIGURE 4. SAGITTAL VIEW OF THE MIRD PHANTOM. THE PHANTOM IS FACING LEFTWARDS. YELLOW - SOFT TISSUE, TURQUOISE - BONE TISSUE, BLUE - AIR.**

The organs affected by cervical brachytherapy are the cervix, uterus, bladder, sigmoid, and rectum. The position, shape, and composition of the organ cells in the MIRD Phantom coordinate space are given in Table 3.

**TABLE 3. EQUATIONS OF 2D-SURFACES THAT DEFINE MAJOR ORGANS CONSIDERED IN THE SIMULATION, AND THE DESCRIPTION OF THE VOLUMES DEFINED BY THOSE SURFACES. UNITS OF LENGTH, WHERE APPROPRIATE, ARE CENTIMETERES.**

| **Organ** | **Shape** | **Boundary Equation** | **Organ Volume Space** |
|---|---|---|---|
| Uterus | Sliced ellipse | (wall): $75.61172\,x^2 + 14.65741(y+1.96)^2 + 192.0081\,(z-12.62)^2 = 461.2995$ (plane): $y = -4.77$ | Inside the wall and to the right of cut-off plane (i.e. $y \geq -4.77$) |
| Bladder | Ellipse | (wall): $110.4979\,x^2 + 176.3504(y+4.41)^2 + 208.2999\,(z-7.21)^2 = 2014.6979$ | Inside the wall |
| Sigmoid | Parts of two tori | (upper torus): $\frac{y^2}{1.18^2} + \frac{\left(\sqrt{(x-2.09)^2+(z-7.86)^2}-5.16\right)^2}{1.76^2} - 1 = 0$ (lower torus): | Inside quarter-circle segments of upper and lower torus, between the place $z = 0$ and $z = 7.86$. |

| | | | |
|---|---|---|---|
| | | $\frac{y^2}{1.18^2} + \frac{\left(\sqrt{(x-2.59)^2+z^2} - 2.70\right)^2}{1.76^2} - 1 = 0$ | |
| Cervix (tumor)[1] | Sphere | (sphere): $x^2 + (y-4.5)^2 + (z-9.915)^2 = 6.25$ | Inside the sphere |

## 2.4 HYPOTHESIS

This work attempted to establish that Ytterbium-169 used for HDR brachytherapy of cervical cancer:

1. Delivers more uniform dose rate to the tumor of the cervix and results in a larger ratio of tumor-to-healthy tissue dose compared to brachytherapy with Iridium-192 source of the same geometry.
2. Delivers an equivalent or smaller dose to the organs at risk, i.e. uterus, bladder, sigmoid, and rectum, as an Iridium-192 source of the same geometry.

The hypothesis was tested using a Monte Carlo simulation conducted with LANL MCNP6 Code. In particular, the simulation was used to compare the doses delivered to a cervical tumor model – a sphere with 2.5 cm radius – and organs at risk by a standard-shaped Ytterbium-169 and

[1] See methodology for placement guidelines.

Iridium-192; construct dose rate intensity plots and dose-volume histograms for the tumor and organs at risk.

# 3 METHODOLOGY

The brachytherapy treatment was modeled with MCNP6, using MIRD Phantom to represent an adult female, and custom-defined geometry to represent HDR brachytherapy radiation sources. Two MCNP simulations were run with identical geometries and different source parameters: one corresponding to a Ytterbium-169, and the other – to the Iridium-192 source. The number of particle histories simulated in each run was $nps = 5000000$. For each run, the dose rate delivered by the radiation sources to the body tissues was estimated using the same 3-dimensional mesh (array-like) tallies that sored the dose rate measurements for every voxel defined in the tally.

If was assumed that, given the energies of the particles involved in the modeled process, photons are the only particles capable of traveling significant distance, while electron produced as a result of photon-tissue interactions were not tracked by the code and were simulated as depositing their whole energy locally.

## 3.1 MIRD PHANTOM

In the MCNP coordinate space, the phantom is oriented upright with the main axis of the cylindrical torso aligned with the z-axis if the coordinate frames. The phantom is facing the negative y-direction. Thus, the coordinate planes represent the following cross-sections of the phantom:

xy-plane – Transverse plane

yz-plane – Sagittal plane

xz-plane – Frontal (or Coronal) plane

## 3.2 HDR BRACHYTHERAPY SOURCE

The brachytherapy source parameters were take from (Medich *et al.,* 2006; Medich and Munro, 2007). The source was modeled as a right cylinder with base radius $r_{sb} = 0.0365\ cm$ and length $h_s = 0.360\ cm$ along the main axis. The source was encapsulated in a stainless steel shell $0.017\ cm$ thick. A $0.010\ cm$ thin air layer was left between the inner seed and the stainless steel encapsulation. The surface cards for the seed assembly were defined in an auxiliary coordinate system, in which the cylindrical source was oriented along the $z'$-axis of the coordinate frame, with the stainless steel shell spanning from $z = 0\ cm$ to $z = 0.414\ cm$.

The auxiliary coordinate system was shifted to position the source in the pelvic area near the posterior side of the uterus, at the hypothetical location of the cervix approximately 2 cm to away from the internal orifice of the uterus. The operations applied to the auxiliary coordinate system to shift it into the its final location are as follows:

1. The origin $O'$ of the auxiliary coordinate frame was translated to the point $p = (0, 4.5, 9.915)$ in the global MCNP coordinate frame.
2. Then, the auxiliary coordinate system was actively rotated around the $x'$-axis over angle $\theta = \frac{\pi}{4}$ as defined by the matrix:

$$R = \begin{pmatrix} 1 & 0 & 0 \\ 0 & \cos\left(\frac{\pi}{4}\right) & -\sin\left(\frac{\pi}{4}\right) \\ 0 & \sin\left(\frac{\pi}{4}\right) & \cos\left(\frac{\pi}{4}\right) \end{pmatrix}$$

As a result of the transformation, the cylindrical seed was positioned such that it's main axis lied entirely in the sagittal plane, at a 45° angle above the hypothetical line of sight of the phantom.

The MCNP code block with the definition of the source is given in Figure 3.

```
(cell card block)
9900 13 -7.80 (-9001 9002) imp:p=1 $ steel shell
9901 2 -0.00129 -9002 9003 imp:p=1 $ air layer inside the seed
9902 11 -6.90 -9003 imp:p=1 $ Y-169 (or Ir-192) seed

(surface card block)
9001 900 rcc 0 0 0 0 0 0.414 0.0635 $ outer shell surface
9002 900 rcc 0 0 0.017 0 0 0.380 0.0465 $ inner shell surface
9003 900 rcc 0 0 0.027 0 0 0.360 0.0365 $ Ytterbium Oxide surface

(transformation card from data card block)
*tr900 0 4.5 9.915 0 90 90 90 45 -45 90 135 45 $ seed position transform
```

**FIGURE 5. BRACHYTHERAPY SOURCE GEOMETRY DEFINITION IN MCNP CODE. IR-192 SEED WAS DEFINED IN THE SAME WAY, WITH A DIFFERENT MATERIAL NUMBER APPLIED IN CELL 9902 DEFINITION. FOR CONVENIENCE, THE SEED GEOMETRY WAS DEFINED IN A SEPARATE COORDINATE SYSTEM, WHICH WAS THEN SHIFTED INTO THE PROPER POSITION VIA A COORDINATE TRANSFORMATION CARD.**

Cell 9902 containing the brachytherapy seed was defined as the only source used in the simulation. For each of the two MCNP runs, cell 9902 was endowed with Ytterbium-169 or Iridium-192 photon emission energy spectrum (both spectra shown in Figure2). The detailed photon energy distributions are shown in Table 4 – for Ytterbium-169, and Table 5 – for Iridium-192. Figure 4 displays the MCNP code used to define the sources in the simulation software.

**TABLE 4. YTTERBIUM-169 PHOTON ENERGY SPECTRUM USED FOR THE MCNP SIMULATION. WEIGHTED AVERAGE ENERGY OF THE SPECTRUM IS 92.7 KEV (MEDICH *ET AL.*, 2006)**

| Energy (keV) | Intensity (%) |
|---|---|
| 49.5 | 53.2 |
| 50.7 | 94.0 |
| 57.6 | 29.5 |
| 59.1 | 8.2 |
| 63.1 | 44.2 |
| 93.6 | 2.6 |
| 109.8 | 17.5 |
| 118.2 | 1.9 |
| 130.5 | 11.3 |
| 177.2 | 22.2 |
| 198.0 | 35.8 |
| 162.1 | 1.7 |
| 307.7 | 10.1 |

**TABLE 5. IRIDIUM-192 PHOTON ENERGY SPECTRUM USED FOR THE MCNP SIMULATION. WEIGHTED ENERGY OF THIS ENERGY SPECTRUM IS 387.5 KEV (MEDICH AND MUNRO, 2007).**

| Energy (keV) | Intensity (keV) |
|---|---|
| 61.49 | 1.20 |
| 63.00 | 2.07 |
| 64.12 | 2.65 |
| 66.83 | 4.53 |
| 71.08 | 0.24 |
| 71.41 | 0.46 |
| 73.36 | 0.16 |
| 75.37 | 0.53 |
| 75.75 | 1.03 |
| 77.83 | 0.37 |
| 136.34 | 0.18 |
| 201.31 | 0.47 |
| 205.80 | 3.30 |
| 283.27 | 0.26 |
| 295.96 | 28.67 |
| 308.46 | 30.00 |
| 316.51 | 82.81 |
| 373.49 | 0.72 |
| 416.47 | 0.66 |
| 468.07 | 47.83 |
| 484.58 | 3.18 |
| 489.04 | 0.44 |
| 588.58 | 4.52 |
| 604.41 | 8.23 |
| 612.47 | 5.31 |
| 884.54 | 0.29 |

```
c     Ytterbium-169 Source
SDEF cel=9902 erg=d1 x=d2 y=d3 z=d4 par=2
SI1 L 0.0495 0.0507 0.0576 0.0591 0.0631 0.0936 &
      0.1098 0.1182 0.1305 0.1772 0.198 0.2611 0.3077
SP1 53.2 94.0 29.5 8.2 44.2 2.6 17.5 1.9 11.3 22.2 35.8 1.7 10.1
SI2 -0.0365 0.0365
SP2 0 1
SI3 4.200 4.507
SP3 0 1
SI4 9.908 10.215
SP4 0 1

c     Iridium-192 Source
SDEF cel=9902 erg=d1 x=d2 y=d3 z=d4 par=2
SI1 L 0.06149 0.06300 0.06412 0.06683 0.07108 0.07141 0.07336 &
      0.07537 0.07575 0.07783 0.13634 0.20131 0.20580 0.28327 &
      0.29596 0.30846 0.31651 0.37349 0.41647 0.46807 0.48458 &
      0.48904 0.58858 0.60441 0.61247 0.88454
SP1   1.20 2.07 2.65 4.53 0.24 0.46 0.16 &
      0.53 1.03 0.37 0.18 0.47 3.30 0.26 &
      28.67 30.00 82.81 0.72 0.66 47.83 3.18 &
      0.44 4.52 8.23 5.31 0.29
SI2 -0.0370 0.0365
SP2 0 1
SI3 0.6 1.1
SP3 0 1
SI4 9.81 10.31
SP4 0 1
```

**FIGURE 7. MCNP SOURCE ENERGY SPECTRUM DEFINITION USED IN THE SIMULATION.**

The composition of materials used to model components of the seed assembly are shown in Table 6.

**TABLE 6. ATOMIC COMPOSITION OF MATERIAL IN BRACHYTHERAPY SEED ASSEMBLY.**

| **Material** | **Atom** | **Atomic Fraction** |
|---|---|---|
| Air<br>(density $\rho_A = 0.00129$ g/cm$^3$) | Nitrogen | 0.80 |
| | Oxygen | 0.20 |

| | | |
|---|---|---|
| Stainless Steel<br><br>(density $\rho_{SS} = 7.80$ g/cm$^3$) | Carbon | 0.0008 |
| | Silicon | 0.0100 |
| | Phosphorus | 0.0005 |
| | Sulfur | 0.0003 |
| | Chromium | 0.1900 |
| | Manganese | 0.0200 |
| | Iron | 0.6859 |
| | Nickel | 0.0925 |
| Ytterbium-169<br><br>(density $\rho_Y = 9.17$ g/cm$^3$) | Ytterbium | 0.40 |
| | Oxygen | 0.60 |
| Iridium-192<br><br>(density $\rho_{Ir} = 22.4$ g/cm$^3$) | Iridium | 0.40 |
| | Oxygen | 0.60 |

The MCNP code with the material definition cards is given in Figure [FIGURE NUMBER].

```
m2    7000 0.8 8000 0.2       $ air
m11   70000.04p 0.4000 8000.04p 0.6000 $ Y-169 oxide (density -9.17)
m12   77000.04p 0.4000 8000.04p 0.6000 $ Ir-192 oxide (density -22.4)
m13   6000.04p 0.0008 14000.04p 0.0100 15000.04p 0.0005 &
      16000.04p 0.0003 24000.04p 0.1900 25000.04p 0.0200 &
      26000.04p 0.6859 28000.04p 0.0925    $ Steel (density -7.80)
```

**FIGURE 8. MATERIAL DEFINITIONS IN MCNP CODE FOR THE MATERIALS USED IN THE SOURCE ASSEMBLY. MATERIAL 1 - AIR, MATERIAL 11 - YTTERBIUM-169 OXIDE, MATERIAL 13 - STAINLESS STEEL.**

## 3.3 TALLIES

The dose rate delivered to tissues in the vicinity of the source was obtained from the MCNP6 Monte Carlo simulation using a Cartesian TMESH tally of type 3. This TMESH tally is a 3-

dimensional array of dose rate values, in units of MeV/($cm^3$ n), delivered to the voxel associated with the array entry. The coordinate boundaries of the voxels corresponding to array entries are defined by the user, and are output in the TMESH output file as three 1-dimensional arrays with coordinates along x-, y-, and z-axis.

The TMESH tally used in the simulation was implementer with 200 bins, spanning from -10 cm to 10 cm along each coordinate direction, with 0.1 $cm$ spacing for each bin, and 0.001 $cm^3$ volume associated with every 3D voxel. The TMESH tally was defined in the coordinate system

```
RMESH123 TRANS 900
   CORA123 -10 199I 10
   CORB123 -10 199I 10
   CORC123 -10 199I 10
ENDMD
```

**FIGURE 9. MCNP6 TMESH TALLY OF TYPE 3 CODE BLOCK. THE SAME TALLY WAS USED FOR SIMULATING BOTH YTTERBIUM-169 AND IRIDIUM-192.**

of the source in the coordinate system associated with the source and shifted along with it via the coordinate transformation card used in defining the source.[2] The same TMESH tally was used for simulating both Ytterbium-169 and Iridium-192. The MCNP6 code block used to define the tally is shown in Figure 9.

The TMESH tally output file was processed with a Python script and the following quantities were obtained:

[2] I.e. the TMESH tally bin grid did not align with the coordinate grid of the system associated with the MIRD phantom.

1. $P = \{p_{ijk} = (x_i, y_j, z_k)\}$ - set of center points of the rectangular voxels defined in the TMESH block in the MCNP6 input file.
2. $V_{ijk} = 0.001\ cm^3$ – voxel volume associated with every point $p_{ijk} \in P$.
3. $I(p_{ijk})$ – dose rate measurements, in units of $MeV/(cm^3 \cdot nps)$, obtained at points $p_{ijk} \in P$.

In addition, the dose rate unit conversion factor $\alpha_{dr}$ for soft tissue was obtained using the soft tissue density $\rho_{st} = 1.04\ g/cm^3$ defined in the MIRD phantom MCNP code:

$$\alpha_{dr} = 1.54056 \cdot 10^{-10}\ (J \cdot cm^3)/(MeV \cdot kg)$$

## 3.4 Dore Rate Intensity

The dose rate function $G(p_{ijk}) = \alpha_{dr}\ I(p_{ijk})$ was renormalized to the dose measured at the prescription point A $p_A = (0, 2, 2)$:

$$G_N(p_{ijk}) = \frac{G(p_{ijk})}{G(p_A)}$$

Renormalized dose rate function $G_N(p_{ijk})$ was plotted in the two planes:

1. Plane transverse to the axis of the cylindrical source, defined by the bases $t_x = (1, 0, 0)$ and $t_y = (0, 1/\sqrt{2}, 1/\sqrt{2})$.
2. Sagittal plane of the phantom displaying the longitudinal cross-section of the source, and defined by the bases

## 3.5 Dose Rate Map

The dose rate function $G(p_{ijk}) = \alpha_{dr}\, I(p_{ijk})$ was renormalized to the dose measured at the prescription point A $p_A = (0, 2, 2)$:

$$G_N(p_{ijk}) = \frac{G(p_{ijk})}{G(p_A)}$$

Renormalized dose rate function $G_N(p_{ijk})$ was plotted ass a heat man in the two planar sections of the MIRD phantom:

3. Plane transverse to the axis of the cylindrical source, defined by the bases $t_x = (1, 0, 0)$ and $t_y = (0, 1/\sqrt{2}, 1/\sqrt{2})$.
4. Sagittal plane of the phantom displaying the longitudinal cross-section of the source, and defined by the bases $l_x = (0, 1, -1)$ and $l_y = (0, -1, 1)$.

Built-in Python linear interpolation was used to find values dose rate values between the points *P* of the mesh.

## 3.6 Dose Volume Histograms

The dose-volume histogram was constructed for the tumor, 5 cm in diameter and centered at the source; and uterus, located approximately 7 cm away from the source (center), with the point of the uterus closest to the source located 2.4 cm away from the source.

For each of the two targets, the histograms were constructed on the following way:

1. A set of points $P_t \subset P$ inside the volume of the target tissue was selected.
2. The relative volume $V_r(D_\delta)$ of the target tissue receiving a dose equal to or above $D_\delta$ was found using the formula:

$$V_r(D_\delta) = \frac{\sum_{p \in P_t} N(G_N(p) \leq D_\delta) \cdot v}{\sum_{p \in P_t} v}$$

where $N(G_N \leq D_\delta)$ is the counting function that returns 1 whenever the condition given as the arguments is satisfied:

$$N(x \leq a) = \begin{cases} 1, & x \leq a \\ 0, & x > a \end{cases}$$

Plots of the relative volume function, or dose volume histograms were constructed for the tumor and uterus from simulations with Ytterbium-169 and Iridium-192.

# 4 RESULTS

The MCNP6 TMESH type 3 tally output was converted into the dose rate and the dose rate function $G_N(x_i, y_j, z_k)$, normalized to the prescription dose at point A was obtained.

## 4.1 DOSE RATE MAP

The MCNP6 TMESH type 3 tally output was converted into the dose rate and the dose rate function $G_N(x_i, y_j, z_k)$, normalized to the prescription dose at point A was obtained. Figure 11 shows the 2-dimensional heat map of the normalized dose rate function $G_N(x_i, y_j, z_k)$ in the plane perpendicular to the main axis of the cylindrical seed at half-seed-length point with $z_k = 0.15$. The schematic drawing of the plane plotted in Figure 11 is shown in Figure 10. The color scheme represent the values attained by $G_N(x_i, y_j,\ z_k = 0.15)$ and arranged in color-coded bins between 0 and 1 prescription doses. The seed is positioned in the center of the plot and is surrounded primarily by soft tissue. Volumes outlined in white are filled with bone tissue.

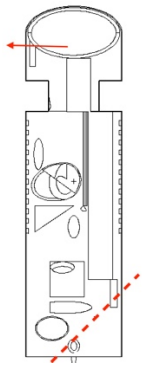

**FIGURE 10. SCHEMATIC DRAWING OF THE MIRD PHANTOM DEPICTING THE PLANE OF THE PLOT AS A DOTTED RED LINE.**

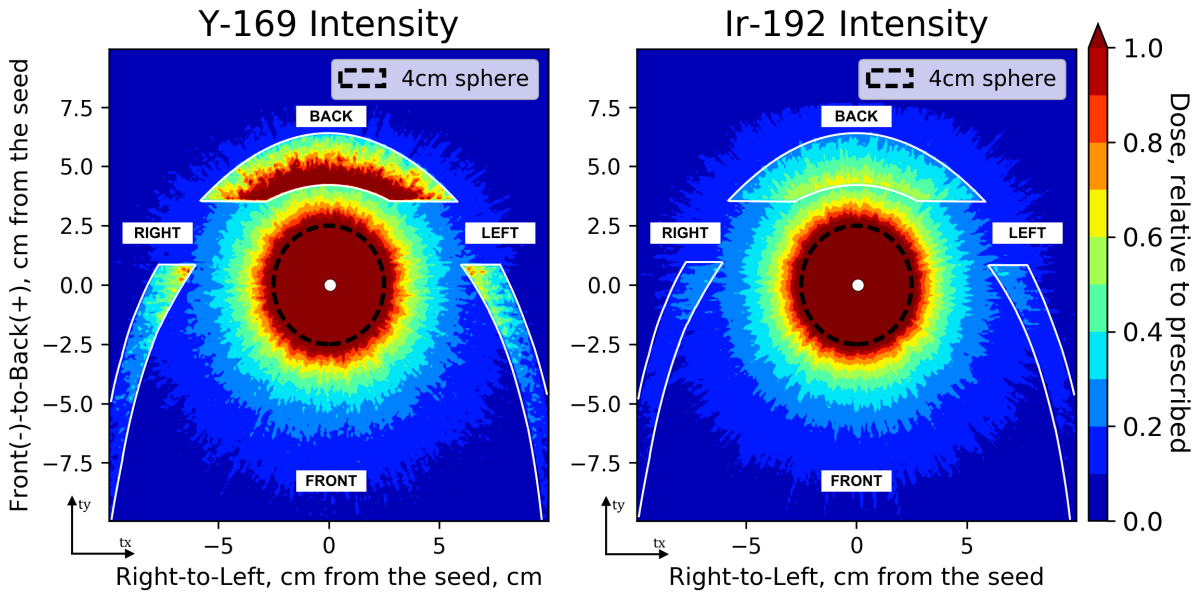


**FIGURE 11. HEAT MAP OF THE DOSE RATE FUNCTION NORMALIZED TO THE PRESCRIPTION DOSE AT POINT A. THE PLANE OF THE PLOT IS TRANSVERSE TO THE BRACHYTHERAPY SEED AND SPLITS THE SEED IN TWO IDENTICAL CYLINDERS. THE WHITE DOT MARKS THE LOCATION OF THE SEED. VOLUMES OUTLINED IN WHITE ARE BONE TISSUE; ALL OTHER VOLUMES SHOWN ON THE PLOT ARE SOFT TISSUE, WITH THE EXCEPTION OF THE SEED.**

As the figure suggests, there the dose rate delivered to the target – tumor of 5 cm radius – was the same for Ytterbium-169 and Iridium-192 seeds, with the tumor receiving at least one prescription dose in all points plotted in this cross-section. Ytterbium-169 delivered a significant dose to the pelvic bone as some of the bone sections closest to the source receiving more than one prescription dose. Iridium-192 delivered a smaller dose to the pelvis which did not exceed 0.7 of the prescription doses.

Similar to the transverse plot, the longitudinal cross-section plot (Figures 12) reveals similar outcomes. Most of the tumor volume received at least the prescription dose with both Ytterbium and Iridium, while Ytterbium-169 delivered a greater dose to the pelvic bone.

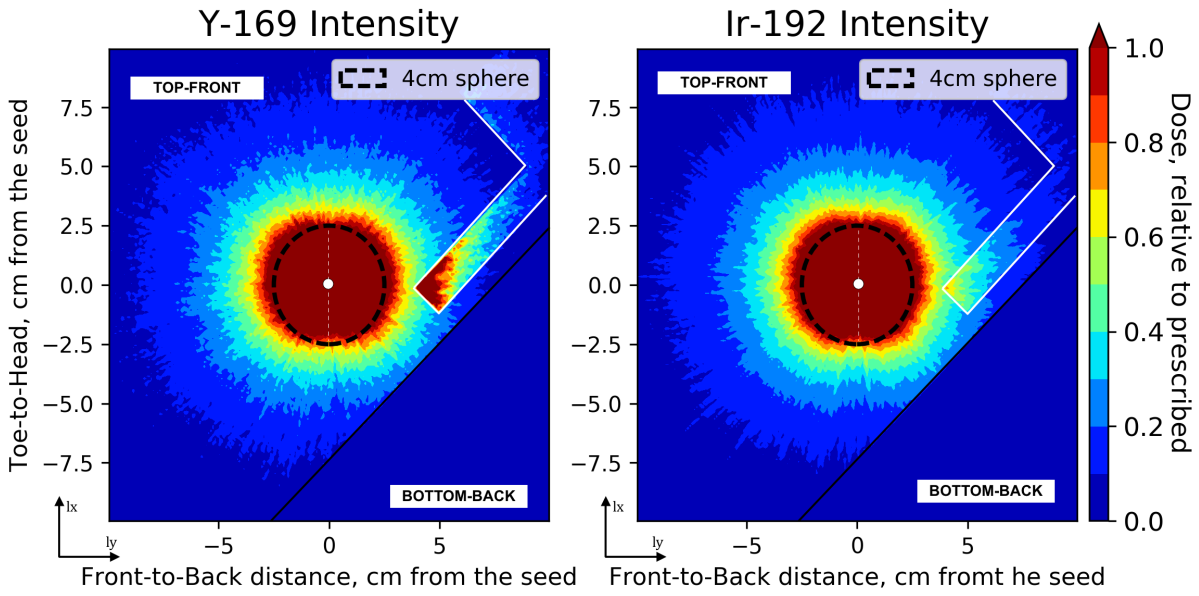


**FIGURE 12. HEAT MAP OF THE DOSE RATE FUNCTION NORMALIZED TO THE PRESCRIPTION DOSE AT POINT A. THE PLANE OF THE PLOT ALIGNS WITH THE SAGITTAL PLANE OF THE PHANTOM AND SPLITS THE BRACHYTHERAPY SEED LONGITUDINALLY, AS SHOWN IN. THE WHITE DOT MARKS THE LOCATION OF THE SEED; WHITE DASHED LINE SHOWS THE AXIS OF THE CYLINDRICAL SOURCE. VOLUMES OUTLINED IN WHITE ARE BONE TISSUE; ALL OTHER VOLUMES SHOWN ON THE PLOT ARE SOFT TISSUE, WITH THE EXCEPTION OF THE SEED.**

## 4.2 DOSE VOLUME HISTOGRAMS

After the normalized dose rate function $G_N(x_i, y_j, z_k)$ was obtained for all tally voxels described by points $P = \{(x_i, y_j, z_k)\}$, the dose volume histograms for the 5 cm spherical tumor and uterus were computed.

Figure 13 shows the dose-volume histogram for the tumor. Ytterbium-169 (blue) performed as well as Iridium-192 (red), delivering at least the prescription dose to almost the entire volume of the tumor phantom.

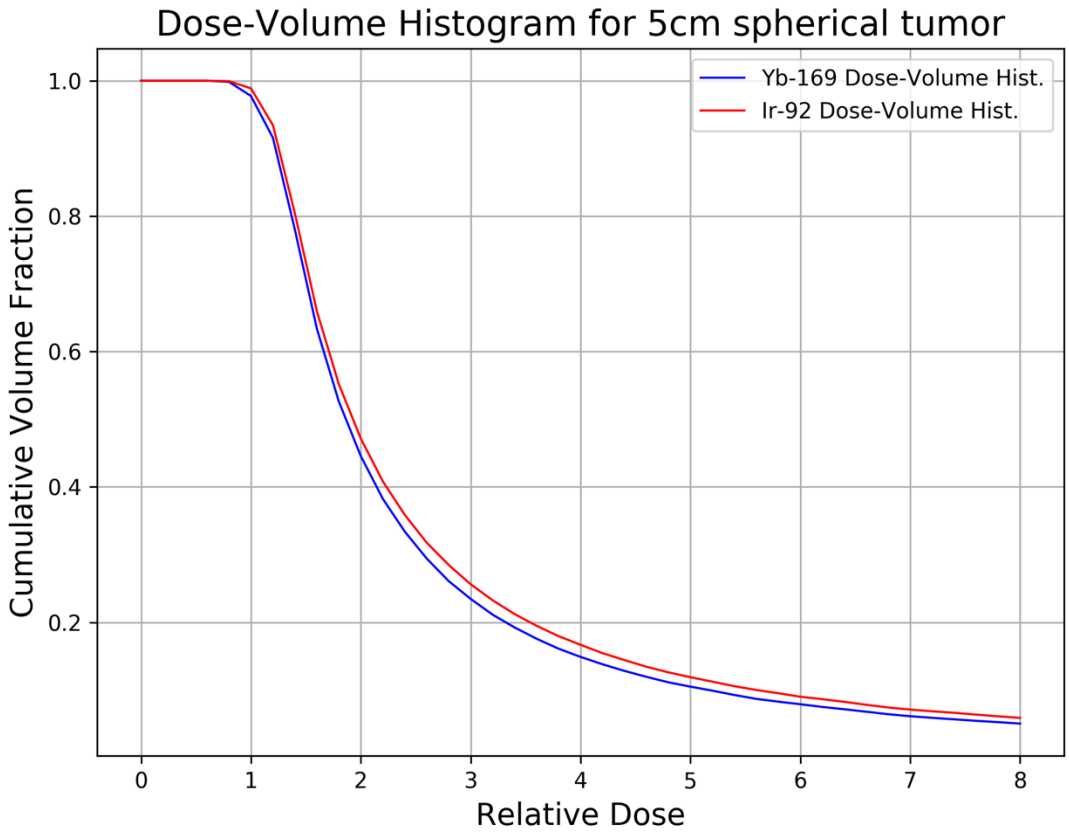


**FIGURE 13. DVH HISTOGRAM FOR 5-CM SPHERICAL TUMOR PHANTOM WITH THE SEED PLACED DIRECTLY IN THE CENTER.**

Figure 14 displays the dose-volume histogram for the uterus. Ytterbium-169 and Iridium-192, as seen from the figure, delivered equivalent doses to the organ. In addition, both sources did not exceed the recommended maximal dose to the organ.

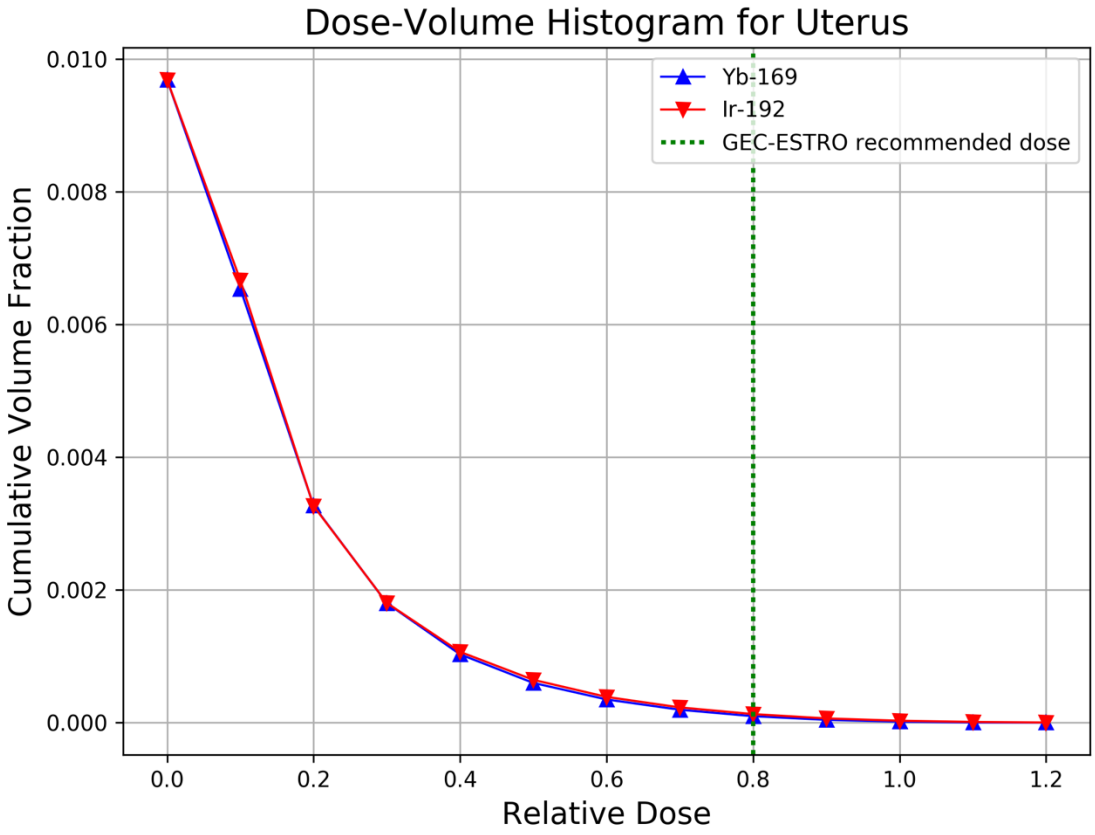


**FIGURE 14. DVH HISTOGRAM FOR THE UTERUS DEFINE IN MIRD PHANTOM.**

# 5 DISCUSSION

Ytterbium-169 is an an attractive target for high-dose rate brachytherapy research as an alternative to Iridium-192. The Monte Carlo simulation analysis of cervical brachytherapy with Ytterbium-169 and Iridium-192 performed in this study suggests that Ytterbium delivers at least

as uniform a dose to soft tissues of the therapeutic target, and an equivalent, dose the uterus – the closest organ at risk – as the current clinical standard Iridium-192.

In contrast to Iridium-192, however, Ytterbium deposits higher doses in the bones near the tumor, most likely due to the photoelectric interactions between its lower energy photons and electrons of Phosphorus, Calcium, and other relatively heavy elements abundant in bone tissue. Due to the high radio-resistance of bone tissue, the negative impact of the increased dose to the bone can be a potential can be outweighed by the advantages in shielding of Ytterbium-169 compared to Iridium-192.

# 6 Conclusion and Future Work

This work investigated using Ytterbium-169 for high-dose rate brachytherapy used in treatments of cervical cancers. It has shown that the dose delivered to the tumor is at least equivalent to that delivered with Iridium-192 without an increase in the dose to the soft-tissue equivalent organs-at-risk.

The lower photon emission energy spectrum of Ytterbium-169 was shown to result in greater dose delivery to the bone tissue – an adverse therapeutic outcome compared to Iridium-192.

Readily shielded photons emitted by Ytterbium-169, however, call for investigation Ytterbium-169 application in intensity-modulated HDR brachytherapy.

# 7 BIBLIOGRAPHY


American Cancer Society, 2016. *Treatment options for Cervical Cancer, by Stage.* Last Accessed April, 2017. Available at: https://www.cancer.org/cancer/cervical-cancer/treating/by-stage.html#references

Banerjee, R. and Kamrava, M., 2014. Brachytherapy in the treatment of cervical cancer: a review. *Int J Womens Health*, *6*, pp.555-564.

Chu, S. Y. F; Ekström, L. P; Firestone, R. B, 1999. "The Lund/LBNL Nuclear Data Search, database version 1999-02-28," http:// nucleardata.nuclear.lu.s.e/nucleardata/toi/index.asp, 1999.

Eifel, P.J., Thoms, W.W., Smith, T.L., Morris, M. and Oswald, M.J., 1994. The relationship between brachytherapy dose and outcome in patients with bulky endocervical tumors treated with radiation alone. *International Journal of Radiation Oncology* Biology* Physics*, *28*(1), pp.113-118.

Goorley, T., et al., 2012. "Initial MCNP6 Release Overview", Nuclear Technology, **180**, pp 298-315.

International Commission of Radiation Units and Measurements, 1985. *Dose and Volume Speci cation for Reporting Intracavitary Therapy in Gynaecology*. Bethesda, MD: ICRU; 1985. Report No: 38.

Jewett, J.W. and Serway, R.A., 2008. *Physics for scientists and engineers with modern physics*. Cengage Learning EMEA.

Lawrence, T.S., Ten Haken, R.K. and Giaccia, A., 2008. Principles of radiation oncology. *Cancer: principles and practice of oncology. 8th ed. Philadelphia: Lippincott Williams and Wilkins*.

Medich, D.C., Tries, M.A. and Munro, J.J., 2006. Monte Carlo characterization of an ytterbium-169 high dose rate brachytherapy source with analysis of statistical uncertainty. *Medical physics*, *33*(1), pp.163-172.

Medich, D.C. and Munro, J.J., 2007. Monte Carlo characterization of the M-19 high dose rate Iridium-192 brachytherapy source. *Medical physics*, *34*(6), pp.1999-2006.

Rijnders, A., 2009. Photon Sources for Brachytherapy. In *Radiotherapy and Brachytherapy* (pp. 185-193). Springer Netherlands.

U.S. Cancer Statistics Working Group, 2016. *United States Cancer Statistics: 1999–2013 Incidence and Mortality Web-based Report.* Atlanta (GA): Department of Health and Human Services, Centers for Disease Control and Prevention, and National Cancer Institute. Available at: http://www.cdc.gov/uscs.

Xu, X.G. and Eckerman, K.F. eds., 2009. *Handbook of anatomical models for radiation dosimetry*. Taylor & Francis.